

Mechanical Control of Cell flow in Multicellular Spheroids

Morgan Delarue,^{1,3} Fabien Montel,² Ouriel Caen,³ Jens Elgeti,⁴ Jean-Michel Siaugue,⁵ Danijela Vignjevic,⁶ Jacques Prost,^{1,7} Jean-François Joanny,¹ and Giovanni Cappello¹

¹*Physicochimie Curie (Institut Curie, CNRS-UMR168, UPMC), Institut Curie, Centre de Recherche, 26 rue d'Ulm, 75248 Paris Cedex 05, France*

²*MSC (Université Paris-Diderot, CNRS-UMR 7057), 5 Rue Thomas Mann, 75013 Paris, France*

³*Université Paris Diderot, 5 Rue Thomas Mann, 75013 Paris, France*

⁴*Institute of complex system and Institute of advanced simulation; Forschungszentrum, Jülich, Germany*

⁵*PESCA (Université Pierre et Marie Curie, UMR 7195), 4 place Jussieu, 75006 Paris, France*

⁶*Institut Curie (UMR 144), Centre de Recherche, 26 rue d'Ulm, 75248 Paris Cedex 05, France*

⁷*Ecole Supérieure de Physique et Chimie Industrielle, 10 rue Vauquelin, 75005 Paris, France*

(Received 27 September 2012; revised manuscript received 26 November 2012; published 26 March 2013)

Collective cell motion is observed in a wide range of biological processes. In tumors, physiological gradients of nutrients, growth factors, or even oxygen give rise to gradients of proliferation. We show using fluorescently labeled particles that these gradients drive a velocity field resulting in a cellular flow in multicellular spheroids. Under mechanical stress, the cellular flow is drastically reduced. We describe the results with a hydrodynamic model that considers only convection of the particles by the cellular flow.

DOI: [10.1103/PhysRevLett.110.138103](https://doi.org/10.1103/PhysRevLett.110.138103)

PACS numbers: 87.19.xj, 87.19.R-, 87.17.Jj, 87.18.Fx

Individual or collective cell migration is observed in a wide range of biological processes, but the origin of the motion is often not completely understood. In embryology, for example, collective migration occurs during morphogenetic transformations, such as dorsal closure or gastrulation [1,2], in the absence of any cell proliferation. In adult mammals, tissue renewing often implies collective cell migration. In the self-renewing of the small intestine, for instance, cell migration proceeds from the crypts, where stem cells actively divide, towards the tips of the villis, where cells undergo apoptosis (programmed cell death) and are delaminated [3]. Whether the cell proliferation gradient is a cause of the collective motion or not is still unclear. Cell migration is also observed in tumors: in response to chemical cues, cancer cells can escape the primary tumor and invade the adjacent stroma either collectively or as a single cell [4]. Intravital imaging of tumors growing in living animals reveals that, especially in highly metastatic cancers, cells move directionally towards the blood vessels [5].

Multicellular spheroids are made of cells cultured in 3D that mimic the cellular context and the physiological gradients found in tumors [6], such as oxygen gradients, or growth factors gradients. In both tumors and multicellular spheroids, these gradients lead to an increase of cell proliferation at the periphery and apoptosis in the center [7], which drives a cell flow. Cell flow in multicellular spheroids was first observed by Dorie and colleagues [8,9]. Using two different approaches, in which either ³H-thymidine stained cells or microspheres were put onto the surface of preformed mouse mammary spheroids, they observed a global convergent cell motion.

In this Letter, we address the question of the influence of mechanical stresses on the cellular flow. We previously observed that the growth rate of a multicellular spheroid is drastically reduced by an external mechanical stress. This effect saturates for a stress of 5000 Pa or larger [10,11]. We also showed that cell division, rather than cell death or cell density, is affected by stress, and mostly reduced in the spheroid center. Here, we propose a hydrodynamic model taking into account the gradient of cell proliferation to describe the cellular flow.

In order to measure the cellular flow, we labeled the peripheral cells with nanobeads and followed their distribution over a week in the presence or in the absence of mechanical stress. Multicellular spheroids were prepared using the mouse colon carcinoma cell line CT26 (ATCC CRL-2638). In order to exert a mechanical stress, a biocompatible polymer, Dextran (MW = 100 kDa, Sigma-Aldrich Co., St. Louis, Missouri) was added to the culture medium after the formation of the spheroids [10,11]. The outermost cell layer of a spheroid was labeled with core-shell nanoparticles (CS) made of a maghemite core surrounded by a silica shell. Fluorescent dyes, such as rhodamine isothiocyanate (RITC) or fluoresceine isothiocyanate (FITC), are embedded in the silica shell during the synthesis thanks to covalent bond formation between amino and isothiocyanate groups. The silica shell surface is further twice functionalized by polyethylenglycol chains to enhance biocompatibility and NH₂ terminations to allow anticancerous agent anchoring [12]. These particles are internalized by endocytosis and accumulate in cells where they remain as clusters [inset of Fig. 1(a)]. We have checked that these CS are neither a cell growth nor death

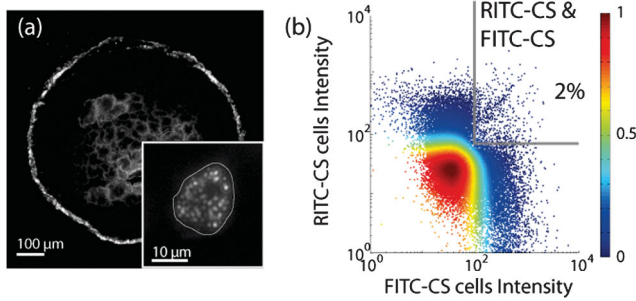


FIG. 1 (color). (a) Cryosection of a spheroid performed directly after labeling with RITC core-shell nanoparticles (RITC-CS). The internal autofluorescence is due to the necrotic core. The inset shows an individual cell with CS clusters. (b) Fluorescence intensity of FITC-CS- and RITC-CS-labeled cells coming from 40 dissociated spheroids, measured by flow cytometry. The color code indicates the density of events. The upper right quadrant corresponds to a cell having both a high number of RITC-CS and FITC-CS, corresponding to less than 2% of the events. 40000 events recorded.

factor, and that they do not change the cell cycle of dividing cells. Spheroids are immersed in the culture medium containing the CS at a concentration of $4 \times 10^{16} \text{ l}^{-1}$ for 1 h at 37°C after which only the outermost cell layer is labeled [Fig. 1(a)]. When a cell divides, the clusters are shared between the two daughter cells.

In order to verify that cells do not interexchange the CS, two different populations of cells were labeled using either FITC-CS or RITC-CS and mixed prior to the formation of

spheroids. After 4 days of growth, the spheroids are dissociated into individual cells, and the fluorescence intensity of individual cells is measured by flow cytometry (FACSsort, Beckman), to assess the number of RITC-CS and FITC-CS clusters per cells. No active exchange of CS has been observed—less than 2% of the recorded events—validating our approach [Fig. 1(b)]. Similar conclusions were drawn for spheroids under mechanical stress. We recorded fluorescent images at the level of the equatorial plane of the spheroids, obtained by cryosections. By sliding a box of width $15 \mu\text{m}$, we calculated the normalized radial distribution of the position of the CS, and not the global intensity.

To separate the effect of the spheroid growth from the purely hydrodynamic cellular flow, we conducted two different experiments. In the first, we used spheroids that have reached their steady-state radius after growing in the presence or in the absence of mechanical stress. After 30 days of growth, spheroids under no mechanical stress and spheroids under 5000 Pa were labeled with RITC-CS. In the second experiment, we used spheroids in their initial growing phase. Right after their formation, they were stained with RITC-CS, and we applied 5000 Pa on half of them. In each case, $N \geq 3$ experiments were done. Figure 2 (top) shows typical spheroid sections either directly after staining (in red) or 4 days later (in green). We observed that, in each case, the stained cells of the spheroids move toward the center.

We begin our analysis with the steady-state spheroids. In the absence of mechanical stress, CS were distributed at

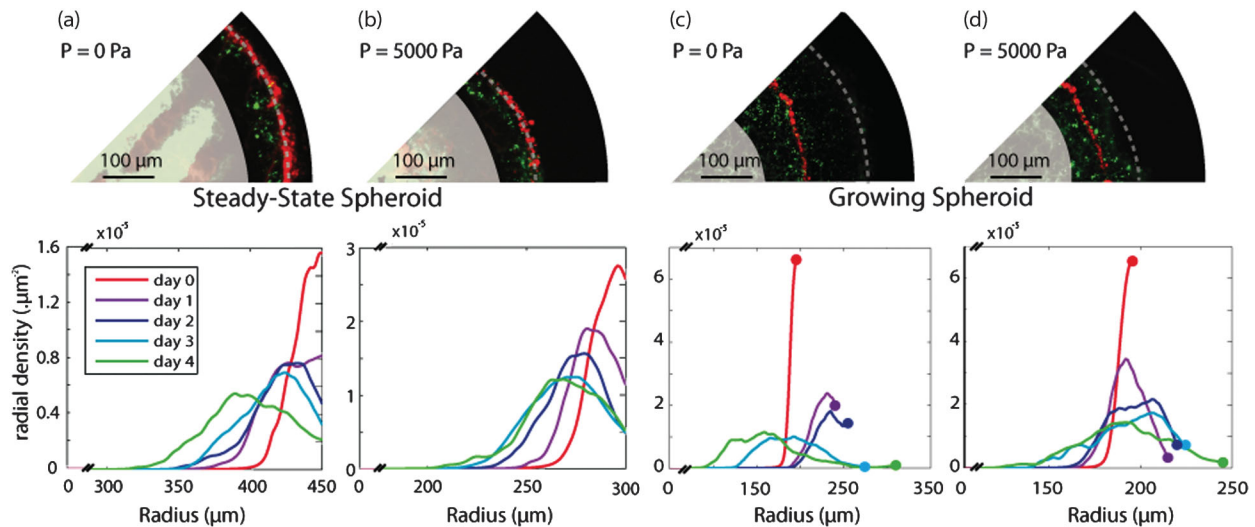


FIG. 2 (color). (a)–(d), (top): Superposition of cryosections of spheroids just after the staining (red) and four days later (green). The dashed line shows the radius at day 4. The autofluorescent core has been hidden for convenience. Bottom: Time evolution of the normalized distribution of RITC-CS-labeled spheroids from day 0 to day 4: red, day 0; purple, day 1; dark blue, day 2; light blue, day 3; green, day 4. (a) and (b): Spheroids at steady state, with no mechanical stress and a steady-state radius of $450 \mu\text{m}$ (a) or under 5000 Pa and a steady-state radius of $300 \mu\text{m}$ (b). (c) and (d) Growing spheroids, with an initial size of $200 \mu\text{m}$, in the absence of mechanical stress (c) or under 5000 Pa (d). The dots indicate the border of the spheroid. Each distribution is the distribution for one spheroid, and each experiment has been repeated $N \geq 3$ times.

the border of the spheroid, with a FWHM of about $20 \mu\text{m}$ [Fig. 2(a)]. Every day the distribution broadened and the maximum moved towards the spheroid center. This result confirms the previous findings of Dorie and co-workers on the existence of a radial convergent flow. In the absence of external mechanical stress, the speed of the maximum was about $25 \mu\text{m day}^{-1}$, consistent with a global convective motion of the cells induced by cell division. When a cell divides in a spheroid at steady state, one of the daughter cells is pushed inside the spheroid. The corresponding displacement would have a velocity of roughly one cell diameter per cell cycle, of order $16 \mu\text{m}/18 \text{h} = 21 \mu\text{m day}^{-1}$, given the measured cell diameter and doubling time of CT26 cells. This is not consistent with cell motion in 3D matrices which has a typical velocity of $1 \mu\text{m min}^{-1}$ for CT26 cells in 3D collagen assay. Under an external stress of 5 kPa, this flow was strongly reduced [Fig. 2(b)] as we estimate a velocity of about $13 \mu\text{m day}^{-1}$, corresponding to a decrease by 50%. Moreover, we observed that the FWHM of the distribution under mechanical stress applied for 4 days was half of the FWHM in the absence of mechanical stress.

We then investigated growing spheroids. Because of the growth, we observed that the CS distribution is moving from the periphery of the spheroid towards its center. In the absence of any applied stress, the maximum of the CS distribution initially followed the border of the growing spheroid [Fig. 2(c)], thus moving away from the center. After day 2, the maximum started to move towards the center. This moving forth and back from the center suggests that, in addition to the observed convergent flow, there is a divergent flow. Under applied mechanical stress, the cellular flow was reduced [Fig. 2(d)]: the maximum of the CS distribution exhibited a much slower drift than in the absence of mechanical stress, and the initial divergent flow seemed impeded.

Several models have been proposed to describe this flow [13–15]. To understand the observed densities, we consider a highly simplified transport model, only taking into account convection. The particle flux is written as $J = v\rho$, where v is the cell velocity and ρ the CS density. Diffusion of the CS can be neglected because they do not leave the cells. In principle, cellular diffusion, originating from the stochasticity of cell proliferation [16], could play a role. However, the diffusion coefficient is of the order of $D = d^2/\tau$, where d is a cell diameter and τ the cell division time; thus, the ratio between the diffusive and convective fluxes is of order d/R , R being the radius of the spheroid. Chemotaxis, as found in Ref. [15], could not be seen in the experiments and is also assumed to be negligible. The transport equation for the particles then reads:

$$\partial_t \rho + \nabla v \rho = 0. \quad (1)$$

Using this minimal model we solve analytically for the particle distribution and extract the growth rate k_g of the spheroids. As described in our previous work, we propose a surface growth model, where there is a surface growth rate increment in a proliferative rim of width λ :

$$k_g = \begin{cases} k \leq 0 & \text{if } r < R(t) - \lambda, \\ k + \delta k \geq 0 & \text{if } r > R(t) - \lambda. \end{cases}$$

k is the bulk growth rate and δk the surface rate increment. As shown in Fig. 3(a), $R(t)$ is the radius of the spheroid at time t , and λ the thickness of the proliferative rim. By writing the mass conservation equation for an incompressible fluid of cells $\nabla v = k(r)$, we obtain the velocity field:

$$v = \begin{cases} \frac{1}{3}kr & \text{if } r < R(t) - \lambda, \\ \frac{1}{3}(k + \delta k)r - \frac{1}{3}\delta k \frac{[R(t) - \lambda]^3}{r^2} & \text{if } r > R(t) - \lambda. \end{cases}$$

In a growing spheroid, the velocity is positive at the periphery of the spheroid and negative close to the center, corresponding to the divergent and convergent flows, respectively [Fig. 3(b)]. When the spheroid is at steady state, $v(R) = 0$, and the velocity is everywhere negative corresponding to a purely convergent flow. At first order in λ/R , we obtain for the radius at steady state $R_\infty = -3\delta k\lambda/k$. Note that if we expand the equation $\frac{dR}{dt} = v(R)$ up to first order, we obtain the same surface growth equation as in Refs. [10,11].

We denote by $\rho_0(r, 0)$ the initial distribution of the CS. Equation (1) can be solved both in the core of the spheroid ($r < R - \lambda$) and in the proliferating rim ($R - \lambda < r < R$):

$$\rho(r, t) = \begin{cases} \rho_0(re^{-kt/3}, 0)e^{-kt} & \text{if } r < R - \lambda, \\ \rho_0(\tilde{r}, 0)e^{-(k+\delta k)t} & \text{if } r > R - \lambda. \end{cases} \quad (2)$$

with $\tilde{r}^3 = e^{-(k+\delta k)t}r^3 + \int_0^t \delta k [R(t') - \lambda]^3 e^{-(k+\delta k)t'} dt'$.

In both regions, the distribution is a function of the initial distribution, modulated by an exponential function. As a

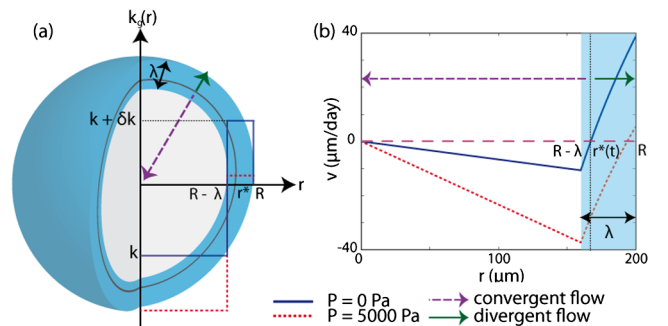


FIG. 3 (color online). Model. (a) Growth rate as a function of position inside the spheroid. (b) Calculated velocity field with the parameters extracted in Table I. Blue, 0 Pa; dashed-red, 5000 Pa; dashed-purple arrow, convergent flow; green arrow, divergent flow.

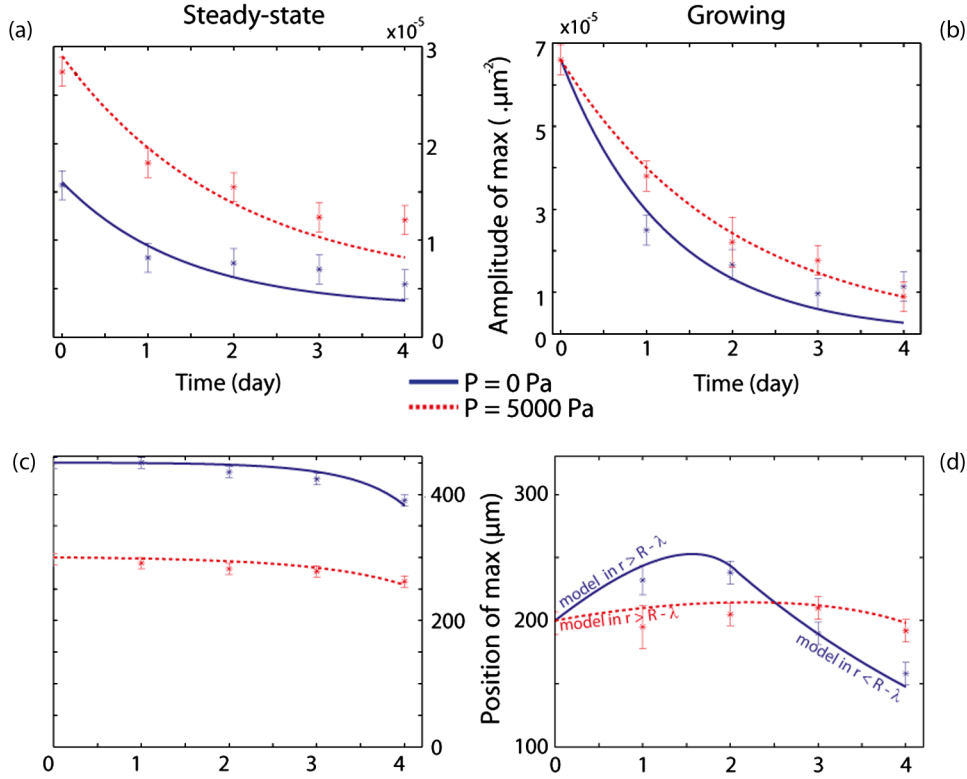


FIG. 4 (color online). Amplitude [(a), (b)] and position [(c), (d)] of the maximum of the CS distribution for steady state [(a), (c)] and growing [(b), (d)]. Solid lines in (a)–(c) are the fitting curves. In (d), solid line is the numerically integrated model, with no adjustable parameter. The error bars correspond to the uncertainty in the evaluation of the position and the amplitude of the maximum for each experiment.

consequence, in the proliferating rim, the maximum decays exponentially in time. We show in Figs. 4(a) and 4(b) the amplitude of the maximum as a function of time, extracted from the data of Fig. 2, for both steady-state and growing spheroids. These data can be readily fitted by an exponential. The fit is not good for the last points, which is consistent with the fact that the distribution enters the $r < R(t) - \lambda$ regime. All the fitted parameters are presented in Table I and our error treatment is explained in the captions. The values of the surface growth rate $k + \delta k$ in the presence or in the absence of mechanical stress are compatible between the growing and steady-state dynamics. We show that under mechanical stress, the growth rate decreases by 30%, which is of the same order of magnitude as the estimated decrease of velocity.

At steady state, the position of the maximum can be written, in the region $r > R_\infty - \lambda$,

$$r(t) = R_\infty [a + (1 - a)e^{[(k + \delta k)t}],$$

with $a = \frac{\delta k}{k + \delta k} [1 - \frac{1}{3}(1 - \frac{k + \delta k}{\delta k})^3]$, where R_∞ and $k + \delta k$ are known parameters. The maximum of the distribution can be readily fitted by this formula, as shown in Fig. 4(c). Therefrom we extract k and δk independently for aggregates at steady state with or without applied mechanical stress. Finally, without any further fitting, we integrate the formulas in Eqs. (2) giving the position of the maximum of the distribution for growing spheroids in both regions, using the same parameters as for spheroids at steady state. Figure 4(d) displays the

TABLE I. Fitting parameters. The uncertainties of the first two columns come from the standard deviation of the fits in Figs. 4(a) and 4(b), whereas the uncertainties for k , δk , and λ are the propagated uncertainties from the measures of R_∞ and $k + \delta k$ and parameter (a) in Fig. 4(c). The rates are in day^{-1} , and the thickness in μm .

P	$(k + \delta k)_{st}$	$(k + \delta k)_{gr}$	k	δk	λ
0	0.7 ± 0.1	0.75 ± 0.1	-0.1 ± 0.2	0.8 ± 0.2	19 ± 38
5000	0.5 ± 0.1	0.5 ± 0.1	-0.3 ± 0.2	0.8 ± 0.2	37 ± 25

calculated values, in very good agreement with the experimental values.

We note that the bulk rate k is close to the values measured in our previous work using a completely different approach and decreases threefold under 5000 Pa. Although it is 40% higher than in Refs. [10,11], we conclude that the surface rate increment δk does not depend much on mechanical stress. The difference in the values of δk comes from the fact that in our previous work we extracted $\delta k\lambda$ and postulated that $\lambda = 70 \mu\text{m}$ from the immunostaining images. Here, λ is written as a function of the growth parameters and the radius in a steady state, and calculated directly. The value of λ is smaller than the postulated $70 \mu\text{m}$. We nevertheless note that the product $\delta k\lambda$ is similar in both works, hence the error on δk . This raises the question of the origin of this thickness, coming either from physiological gradients or mechanical gradients, as suggested in our previous work.

To conclude, we have observed and quantified the influence of mechanical stress on cellular flow in multicellular spheroids, both at steady state and for growing spheroids. The model involving purely convection fluxes is in excellent agreement with our experimental data, which validates the fact that both diffusion and chemotaxis are negligible. This confirms the surface growth model that we previously proposed for a completely different set of experiments.

Even though multicellular spheroids lack vascularization, we postulate that their mechanical properties are comparable to those of vascularized tumors. For instance, it has been shown recently that growing tumors are under both an internal stress induced by growth and an external stress created by the microenvironment [17]. Because of this stress, lymphatic and blood vessels inside the tumor collapse, leading to a tumor with a more efficient vascularization at its surface. Moreover, mechanical stress can affect drug delivery in the tumor, being efficient if the drug penetrates in the central region where the cell flow is convergent. In that case, the drug can be advected by the cell flow in the rest of the tumor, enhancing treatment efficacy.

We would like to thank E. Farge for useful discussions. F.M. and G.C. would like to thank the Axa Research Fund and CNRS for funding. The group belongs to the CNRS consortium CellTiss.

-
- [1] Y. Toyama, X. G. Peralta, A. R. Wells, D. P. Kiehart, and G. S. Edwards, *Science* **321**, 1683 (2008).
 - [2] P. Pouille, P. Ahmadi, A. Brunet, and E. Farge, *Sci. Signal. (Online)* **2**, ra16 (2009).
 - [3] P. Kaur and C. Potten, *Cell and Tissue Kinetics* **19**, 601 (1986).
 - [4] E. T. Roussos, J. S. Condeelis, and A. Patsialou, *Nat. Rev. Cancer* **11**, 573 (2011).
 - [5] J. Condeelis and J. E. Segall, *Nat. Rev. Cancer* **3**, 921 (2003).
 - [6] R. M. Sutherland, *Science* **240**, 177 (1988).
 - [7] F. Hirschhaeuser, H. Menne, C. Dittfeld, J. West, W. Mueller-Klieser, and L. A. Kunz-Schughart, *J. Biotechnol.* **148**, 3 (2010).
 - [8] M. J. Dorie, R. F. Kallman, D. P. Rapacchietta, D. V. Antwerp, and Y. R. Huang, *Exp. Cell Res.* **141**, 201 (1982).
 - [9] M. J. Dorie, R. F. Kallman, and M. A. Coyne, *Exp. Cell Res.* **166**, 370 (1986).
 - [10] F. Montel, M. Delarue, J. Elgeti, L. Malaquin, M. Basan, T. Risler, B. Cabane, D. Vignevic, J. Prost, G. Cappello, and J.-F. Joanny, *Phys. Rev. Lett.* **107**, 188102 (2011).
 - [11] F. Montel, M. Delarue, J. Elgeti, D. Vignevic, G. Cappello, and J. Prost, *New J. Phys.* **14**, 055008 (2012).
 - [12] T. Georgelin, S. Bombard, J. M. Siaugue, and V. Cabuil, *Angew. Chem., Int. Ed. Engl.* **49**, 8897 (2010).
 - [13] D. L. S. McElwain and G. J. Pettet, *Bull. Math. Biol.* **55**, 655 (1993).
 - [14] K. E. Thomson and H. M. Byrne, *Bull. Math. Biol.* **61**, 601 (1999).
 - [15] G. J. Pettet, C. P. Please, M. J. Tindall, and D. L. S. McElwain, *Bull. Math. Biol.* **63**, 231 (2001).
 - [16] J. Ranft, M. Basan, J. Elgeti, J. F. Joanny, J. Prost, and F. Jülicher, *Proc. Natl. Acad. Sci. U.S.A.* **107**, 20863 (2010).
 - [17] J. M. Tse, G. Cheng, J. A. Tyrrell, S. A. Wilcox-Adelman, Y. Boucher, R. K. Jain, and L. L. Munn, *Proc. Natl. Acad. Sci. U.S.A.* **109**, 911 (2012).